A further example in Sec. VIII uses the modified Newtonian theory technique to investigate the static stability of the Apollo Command Module. Using tunnel results from $\theta = 0$ and $\theta = 30°$ only, the static stability conditions of the module are derived and are found to be close to those obtained using the full range of experimental results.

References

[1] Jaslow, H., "Aerodynamic Relationships Inherent in Newtonian Impact Theory," *AIAA Journal*, Vol. 6, No. 4, April 1968, pp. 608–612.

[2] Pike, J., "The Lift and Drag of Axisymmetric Bodies in Newtonian Flow," *AIAA Journal*, Vol. 7, No. 1, Jan. 1969, pp. 185–186.

[3] Pike, J., "Newtonian Lift and Drag of Blunt Cone-Cylinder Bodies," *AIAA Journal*, Vol. 10, No. 2, Feb. 1972, pp. 176–180.

[4] Pike, J., "Newtonian Aerodynamic Forces from Poisson's Equation," *AIAA Journal*, Vol. 11, No. 4, April 1973, pp. 499–504.

[5] Hobson, E. W., *The Theory of Spherical and Ellipsoidal Harmonics*, Cambridge University Press, Cambridge, England, 1931.

[6] Jones, D. J., "Tables of Inviscid Supersonic Flow about Circular Cones at Incidence $\gamma = 1.4$," AGARD-AG-137-71, Dec. 1971.

[7] Babenko, K. I., Voskresenskiy, G. P., Lyubimov, A. N., and Rusanov, U. V., "Three-Dimensional Flow of Ideal Gas past Smooth Bodies," TT F-380, April 1966, NASA.

[8] Beecham, L. J. and Titchener, I. M., "Some Notes on an Approximate Solution for the Free Oscillation Characteristics of Non-Linear Systems typified by $\ddot{x} + F(x, \dot{x}) = 0$," R & M 3651, 1971, Aeronautical Research Council, London, England.

[9] Moseley, W. C., Jr., Moore, R. H., Jr., and Hughes, J. E., "Stability Characteristics of the Apollo Command Module," TN D-3890, March 1967, NASA.

SEPTEMBER 1974 AIAA JOURNAL VOL. 12, NO. 9

Velocity Distribution Functions Near the Leading Edge of a Flat Plate

MANFRED BECKER*
DFVLR, Porz-Wahn, F.R. Germany

AND

FRANK ROBBEN† AND ROBERT CATTOLICA‡
University of California, Berkeley, Calif.

The electron beam fluorescence technique has been used to determine the velocity distribution function within several mean free paths of the leading edge in a rarefied hypersonic helium flow. The Doppler shift and broadening of the 5016 Å He line was measured with a computer controlled Fabry-Perot interferometer. For analysis, the velocity distribution function was approximated with a bimodal model consisting of two Gaussian functions, which was convoluted with the appropriate instrument function and natural line profile and then fitted to the experimental data. Macroscopic properties in the vicinity of the leading edge, slip velocities, and temperature jumps have been obtained from the complete velocity distribution functions.

Nomenclature

A = height of distribution function
c = speed of light
D = orifice diameter
H = enthalpy
k = Boltzmann constant
$L(\lambda)$ = natural line shape of the He 3^1P-2^1S transition
M = Mach number
$M(\lambda, T)$ = Maxwellian distribution function
$\dot{m}$ = mass flow
m = atomic mass of helium
n = weighting of distribution function
p = pressure
R = gas constant
S = speed ratio
$S(\lambda)$ = spectral profile
T = temperature
u = particle velocity
U = mean velocity
ΔU = $U_1 - U_2$
x = axial distance from leading edge
y = height above flat plate
z = direction normal to flow in plane of plate surface
α = energy accommodation coefficient
β = bevel angle
λ = mean free path
λ = wavelength
λ_0 = He 5016 Å wavelength
$\Delta\lambda$ = deviation $\lambda - \lambda_0$
η = coefficient
μ = viscosity
ρ = density
σ = tangential momentum accommodation coefficient

Presented as Paper 73-691 at the AIAA 6th Fluid and Plasma Dynamics Conference, Palm Springs, Calif., July 16–18, 1973; submitted December 27, 1973. This work was done at the University of California, Berkeley, Calif., Department of Mechanical Engineering and was supported in part by the National Science Foundation. The authors gratefully acknowledge the possibility of exchange for the first author worked out between the University of California at Berkeley and the DFVLR, Porz-Wahn, West Germany, which was greatly facilitated by the support of L. Talbot. C. Hansen and G. Lewis skillfully provided the models and other necessary equipment. For the development and operation of the bimodel data reduction program, P. Chen deserves special thanks.

Index category: Rarefied Flows.

* Branch Manager, Angewandte Gasdynamik. Member AIAA.

† Associate Professor in Residence, Mechanical Engineering Department.

‡ Assistant Research Engineer, Fluid Mechanics Laboratory. Associate Member AIAA.

Subscripts

bf	= body-freestream
c	= chamber conditions
g	= gas
w	= wall
x	= axial direction of flow
y	= direction normal to plate surface
z	= direction normal to flow in plane of plate surface
0	= stagnation condition
∞	= freestream condition
1, 2	= class of particles

I. Introduction

THE leading edge of a flat plate in a hypersonic flow has been analyzed extensively. Integral and finite-difference methods have been used in the continuum approaches by Oguchi,[1] Chow,[2] Shorenstein and Probstein,[3] Rudman and Rubin,[4] and Hirschel.[5] The kinetic theory solutions of Huang and Hwang[6] and the Monte Carlo simulation technique of Vogenitz, Broadwell, and Bird[7] have been applied successfully from the free molecular flow limit.

Recent experimental investigations dealt with two special problems. Dyer and Smith[8] and De Geyter, Smolderen, and Wendt[9] observed the upstream density perturbation ahead of the leading edge. Becker[10] has examined the accommodation of the particles at the wall at high energies.

In the present experimental work observations of the velocity distribution function in the immediate vicinity of the leading edge and the wall of a flat plate in a rarefied hypersonic helium flow are presented. In addition to the macroscopic properties in the general flowfield near the leading edge which have been determined from the velocity distribution functions, the velocity slip and temperature jump at the wall have also been determined and are reported in this paper.

II. Apparatus

The helium flowfield was generated by a freejet expansion from a 25.4-mm-diam orifice with stagnation temperature of 296°K and stagnation pressure of 10 torr. The Mach number was approximately 9, the freestream pressure 0.0025 torr, and the freestream temperature 10.7°K. Table 1 gives more detailed information of the flow conditions at the leading edge. The flowfield near the centerline of the freejet can be calculated with the relations given by Ashkenas and Sherman.[11]

The flat plate models for the present investigation were manufactured from copper with a bevel angle of 20° and a leading-edge sharpness of 0.04 mm. The models were 50.8 mm long and 25.4 mm wide. The flat plate was maintained at 290°K by an internal circulating water system and monitored with thermocouples. The flat plate models were mounted on the centerline of the freejet about 130 mm downstream of the orifice.

Table 1 Flow conditions at the leading edge

Stagnation pressure	$P_0 = 10$ torr $= 1330$ N/m^2
Stagnation temperature	$T_0 = 296$°K
Orifice diameter	$D = 25.4$ mm
Mass flow	$\dot{m} = 0.628$ g/sec
Mach number	$M_\infty = 8.93$
Pressure	$p_\infty = 0.002535$ torr
Temperature	$T_\infty = 10.7$ K
Density	$\rho_\infty = 1.52 \cdot 10^{-5}$ kg/m^3
Mean free path	$\lambda_\infty = 1.286$ mm
Velocity	$U_\infty = 1723$ m/sec
Gradient 10 mm	$dM_\infty/M_\infty = 5\%$
Chamber pressure	$p_c = 0.041$ torr
Maximum Mach number	$M_{\infty,\max} = 14.6$
Model temperature	$T_w = 290$°K
Model length	50.8 mm
Model width	25.4 mm
Bevel angle	$\beta = 20°$

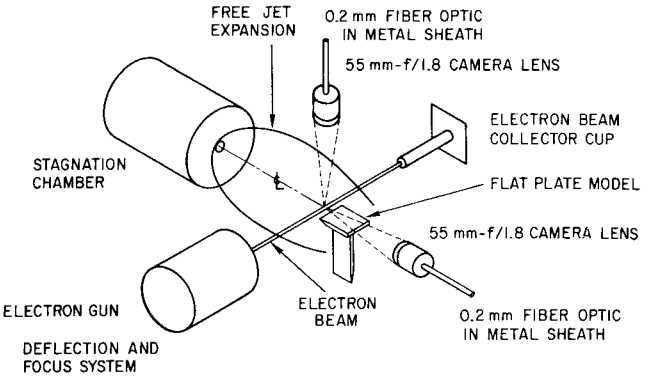

Fig. 1 Electron beam experimental apparatus in low density wind tunnel.

A 27 kv electron beam, with 2–5 ma current and about 1.5 mm in diam was used to induce fluorescence in the helium flowing through the electron beam. The radiation from the fluorescence at a point along the electron beam could be observed with optics aligned parallel and perpendicular to the axis of the jet, as shown in Fig. 1. Fiber optics were used to transmit the light to the Fabry-Perot interferometer. The measurement volume consisted of the intersection of the image of the fiber, about 1.0 mm diam, and the 1.5 mm electron beam diameter. While this measurement volume could be positioned to a precision of 0.025 mm, the accuracy relative to the leading edge of the flat plate was about 0.2 mm.

The Doppler shift and broadening of the 5016 Å helium fluorescence was measured with a piezoelectrically scanned Fabry-Perot interferometer, controlled by a small computer. The spectrum was measured at 100 discrete points, displayed on an oscilloscope, and recorded on punched paper tape. Figure 2 shows typical raw spectra.

A detailed description of the interferometer system, the electron gun, and the wind tunnel is given by Cattolica.[12]

III. Experimental Analysis

The fundamentals of the analysis of the Doppler shift and broadening are discussed by Muntz.[13] Basically, the velocity u

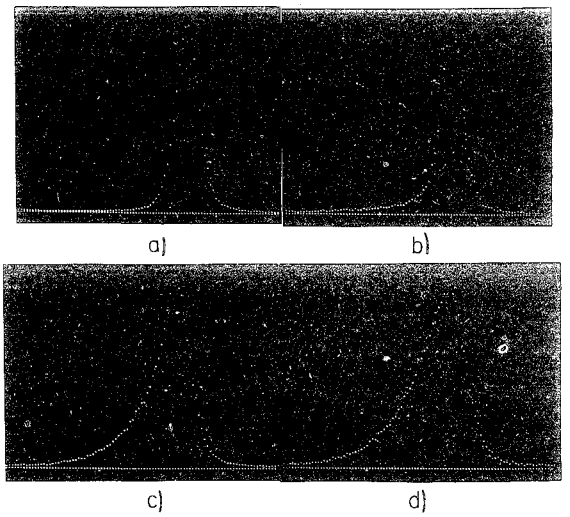

Fig. 2 Development of the axial distribution function along the flat plate: a) $x/\lambda_\infty = -20$, $y/\lambda_\infty = 0$, $T_g = 14$°K; b) $x/\lambda_\infty = -2$, $y/\lambda_\infty = 0$, $T_g = 54$°K; c) $x/\lambda_\infty = 5$, $y/\lambda_\infty = 2$, $T_g = 112$°K; d) $x/\lambda_\infty = 10$, $y/\lambda_\infty = 2$, $T_g = 136$°K.

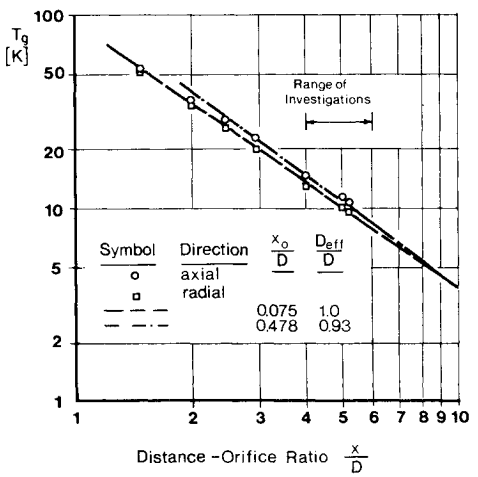

Fig. 3 Temperatures in the freejet with an orifice diameter of 25.4 mm.

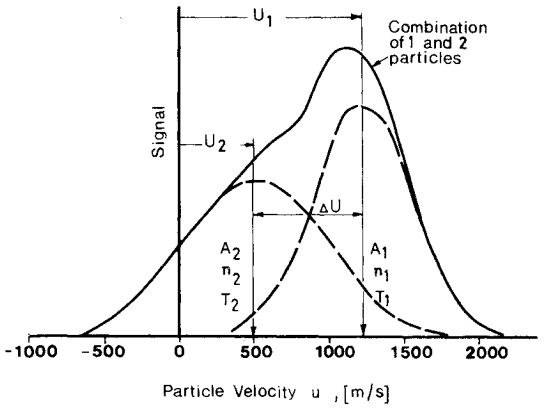

Fig. 4 Bimodal representation of the axial velocity distribution near the surface of the flat plate.

is recorded as a wavelength shift $\Delta\lambda$ according to the relation $u/c = \Delta\lambda/\lambda_0$.

An example of the type of measurement which is obtained with this experimental technique is illustrated by the freestream axial spectral profile shown in Fig. 2a. This spectral profile can be modeled by the following convolution

$$S(\lambda) = \int_{-\infty}^{+\infty}\int_{-\infty}^{+\infty} T(\lambda-\lambda')L(\lambda'-\lambda'')M(\lambda', T)\,d\lambda''\,d\lambda' \qquad (1)$$

where $T(\lambda-\lambda')$ is the interferometer transfer function. $L(\lambda'-\lambda'')$ is the natural line shape of the 5016 Å radiation from the Helium 3^1P-2^1S transition and $M(\lambda', T)$ is a Maxwellian velocity distribution function expressed in terms of the wavelength

$$M(\lambda', T) = \exp\left[-(\lambda'-\lambda_x)^2/\eta T\right] \qquad (2)$$

where $\eta = (\lambda_0{}^2/c^2)(2k/m)$, and $\lambda_x = \lambda_0(1-U_x/c)$. The temperature of 14°K for Fig. 2a is obtained by performing the convolution (1) and iterating on the temperature and U_x until the error between the model and the data is bounded by the statistical error in the data.

The results of flow surveys in the freejet without the flat plate model are shown in Fig. 3, where axial and radial temperatures are presented. The slight translational nonequilibrium which is present should not affect the basic interaction of the flat plate with the flowfield. At the position of the flat plate model in the freejet a gradient in Mach number of 5% over 10 mm in the axial direction and 0.5% in the radial direction is encountered. The small radial flow gradient in the freejet should have a negligible effect on the flowfield interaction with the model and can be neglected. In order to compensate for the influence the axial flow gradient may have in the flow development over the model, the experimental data are normalized by the corresponding freestream conditions.

In the presence of the model (which was maintained at 290°K) the temperatures in the flowfield in the vicinity of the flat plate were substantially higher and the velocity distributions non-Maxwellian. Figure 2 illustrates the non-Maxwellian development of the distribution function along the flat plate. Figure 2a shows the axial distribution of the undisturbed freestream 20 λ_∞ ahead of the flat plate. In Figure 2b, at $2\lambda_\infty$ upstream of the leading edge, the broadening of the low velocity tail of the distribution function results from the upstream influence of particles scattered from the plate. In Figs. 2c and 2d, downstream of the leading edge, the portion of particles in the distribution function which have interacted with the wall and have been thermalized has increased significantly. The distribution functions normal to the plate, which are not shown here, indicate a small mean velocity away from the plate.

To analyze the non-Maxwellian behavior the velocity distribution function was approximated by the sum of two Gaussian, or Maxwellian functions with arbitrary height, width, and position as shown in Fig. 4. This was suggested by the bimodal model, such as has been used for shock wave analysis, except that neither the temperature (width) nor velocity (position) of either function was assumed independent of spatial position, or even of the three axes of observation of a given position. In other words, the distribution function along each axis of observation was approximated by a reasonable function with six adjustable parameters. For comparison with the experimental spectrum the convolution defined by Eq. (1) was used with the single Maxwellian distribution $M(\lambda, T)$ replaced by the two Maxwellians. The six parameters were then determined by

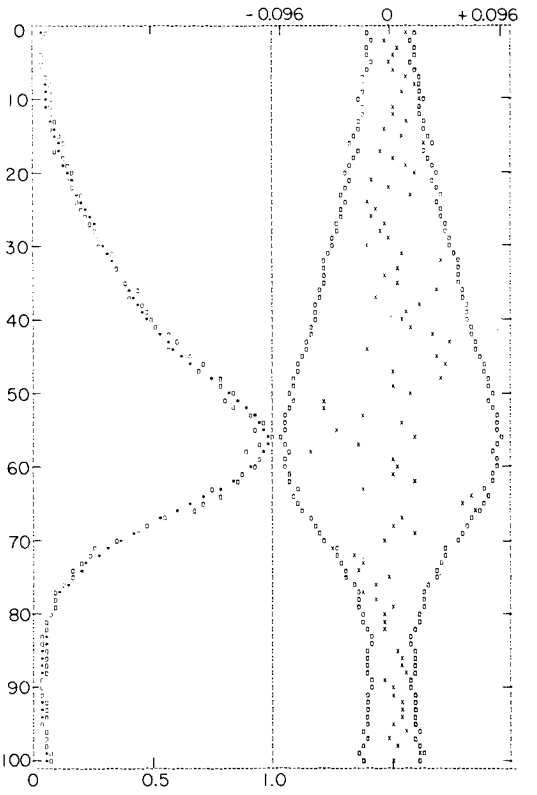

Fig. 5 Example of the comparison of the experimental data (□) with the convolved (*) bimodal representation of the velocity distribution function. The right-hand side gives the error (X) between the experimental measurement and the generated fit, with the outer set of points (□) representing ± three standard deviations, both have been normalized by the peak intensity. Axial distribution function at $x = 31.7$ mm and $y = 1.25$ mm, $T_1 = 90$°K, $T_2 = 295$°K, $A_2/A_1 = 0.45$, $\Delta U = 996$ m/sec, $T_g = 221.4$°K.

searching for an acceptable fit between the experimental spectrum and the convolution given by Eq. (1). This was done on a large computer, by examining line printer plots of the spectrum and the difference between the experimental and calculated spectrum. An example of such a plot, with an acceptable fit, is shown in Fig. 5. Error bounds of three standard deviations are indicated on the plot of the difference, and in general all fits were within such bounds.

The fitting procedure was as follows. The computer program fixed the maximum height and, from the half height points, centered the calculated and experimental spectra. This left four parameters to be determined, T_1, T_2, $\Delta U = U_1 - U_2$, and A_1/A_2. Successive variation of these four parameters was used, systematically varying one or two parameters at a time, until the locus of "best" values was achieved. Since these parameters varied in a smooth manner from point to point through the flowfield, it was possible to obtain quite close fits to the experimental spectra after only a few iterations.

The mean velocity and mean energy for the distribution function were determined by taking the proper moment. We will denote the mean energy by mean temperature in the following, even though temperature is strictly defined only for an equilibrium distribution (which these are certainly not!). The mean velocity U is given by

$$U = \frac{n_1}{n_1+n_2} U_1 + \frac{n_2}{n_1+n_1} U_2 \tag{3}$$

and the temperature T by

$$T = \frac{n_1}{n_1+n_2} T_1 + \frac{n_2}{n_1+n_2} T_2 + \frac{n_1 n_2}{(n_1+n_2)^2} \frac{\Delta U^2}{R} \tag{4}$$

Both the velocity and temperature can be independently determined for each of the three directions x, y, and z, thus the over-all gas temperature T_g is given by

$$T_g = (T_x + T_y + T_z)/3 \tag{5}$$

where T_x, T_y, and T_z are obtained from Eq. (4) applied to the appropriate direction. Zero velocity was determined from the radial distribution (y-direction) in the freestream ahead of the plate.

IV. Results

Measurements of the x and y components of the velocity distribution function were made covering the entire flowfield, from near the plate to the freestream in the y-direction, and from upstream of the leading edge to 31.7 mm downstream of the leading edge. Measurement of the z component of velocity required that the electron beam be normal to the plate, for which another plate with three holes for the electron beam at $x = 19$, 31.7, and 44.3 mm was used. Upstream of the plate z components corresponding to the positions of the x and y components were measured.

To the accuracy of the measurements, it was possible to approximate the x and y distributions at a given point with the same two temperatures T_1 and T_2 and the same density ratio n_1/n_2. The y component distribution was consistent with a small ΔU_y near the leading edge of the plate, but a satisfactory representation could be achieved with $\Delta U_y = 0$ over the whole flowfield. The result near the leading edge is reasonable since the hotter molecules reflected from the plate will be moving away from the plate, while the cold "freestream" molecules will have no mean y velocity.

Downstream of the leading edge at $x = 19$ and 31.7 mm, the z component of the velocity distribution could also be fitted satisfactorily with the same T_1, T_2, and n_1/n_2 as the x and y components, and with $\Delta U_z = 0$. Thus downstream of the leading edge the over-all distribution function at a point is acceptably fit, to the accuracy of these measurements, by a bimodal model with the temperatures T_1, T_2, velocity difference ΔU_x, and density ratio n_1/n_2. However, upstream of the leading edge the z component of the velocity distribution could not be fit satisfactorily with the same T_1, T_2, and n_1/n_2 as the x and y components.

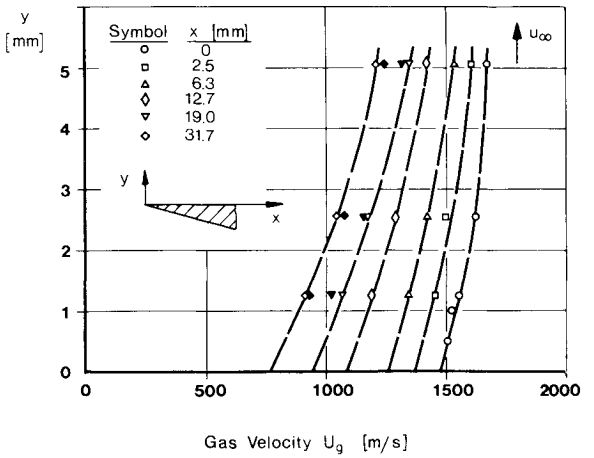

Fig. 6 Velocities in the flowfield above the flat plate. The filled symbols are from x and z measurements with the electron beam normal to the plate.

Even here the deviations were rather small, and it was not possible to clearly identify the trends in these parameters. Data far out from the plate, in the merged boundary layer and shock layer, were not analyzed.

The results which are presented in the remainder of this paper are measurements taken downstream of the leading edge and relatively close to the plate. The axial, or x velocities are shown in Fig. 6 and the gas temperatures T_g are shown in Fig. 7, plotted vs height y and parameterized by axial distance x. The values derived from measurements with the electron beam normal to the plate at $x = 19$ and 31.7 mm, which gave the x and z distributions instead of the x and y, are shown as blackened symbols and are in good agreement. Since the experimental data could be satisfactorily fit within a finite range of the parameters T_1, T_2, ΔU, and A_1/A_2, the sensitivity of the over-all temperature and velocity to these parameters was checked. It was found that the variation in the temperature and velocity was not more than the size of the symbols in Figs. 6 and 7; thus, we believe that the analysis technique is adequate in representing the macroscopic parameters of the distribution functions. The principal errors in the experiment should lie in the experimental spectra and the position of the measurement.

The possible influence of electrons scattered from the wall was considered negligible because (except for one data point) the nearest position of the beam to the wall was larger than the

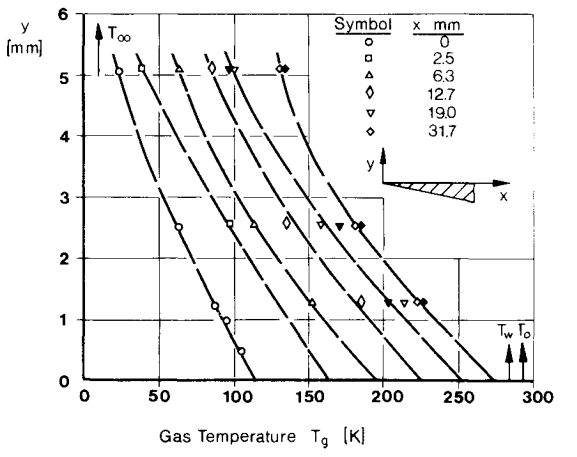

Fig. 7 Temperatures in the flowfield above the flat plate. The filled symbols are from x and z measurements with the electron beam normal to the plate.

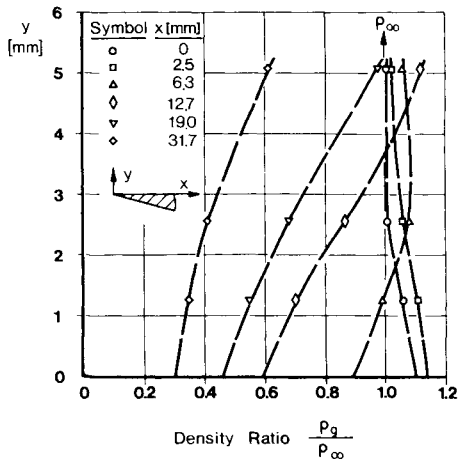

Fig. 8 Densities in the flowfield above the flat plate.

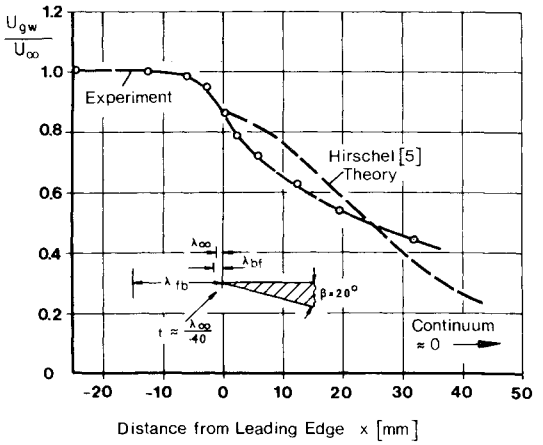

Fig. 10 Velocities extrapolated to the wall, giving the velocity slip and comparison with Hirschel's continuum theory calculations.

beam radius. An influence of this kind could have had severe implications, as the results of Schweiger, Wanders, and Becker[14] have shown.

Figure 8 shows the densities normalized to the freestream density at the same position without the presence of the flat plate. A presently unexplained error in the helium electron beam fluorescence technique, which was first noted by Robben and Talbot,[15] became obvious in these density measurements. There it was found that a shock wave in a freejet expansion of helium was preceded by a small drop in the fluorescence intensity, where no drop in density is expected. Likewise, a drop in intensity was noted upstream of the flat plate, where other measurements indicate a rise in density.[8,9] The reason for this has not been determined, but is presently thought to be connected with trapped resonance radiation. The degree to which this phenomenon has affected the measurements is unknown, but it is thought to be important only upstream of the leading edge, principally affecting the density measurement.

Current analyses of rarefied leading edge flow are based on mean free path arguments, and several mean free paths have been used. The freestream mean free path λ_∞ is defined by

$$\lambda_\infty = (\pi R T_\infty/2)^{1/2}\mu_\infty/p_\infty \tag{6}$$

and has the value of 1.3 mm at the leading edge. The viscosity was calculated following Keesom[16]

$$\mu = 0.5023 \times 10^{-6} T^{0.647} [kgm^{-1}s^{-1}] \tag{7}$$

which holds for the temperature region under investigation between 10 and 300°K. In near free molecule flow a more appropriate mean free path is that of molecules reflected from the body and penetrating into the freestream. Following Hamel and Cooper,[17] for diffuse reflection this is given by

$$\lambda_{bf} = 2(T_w/\pi T_\infty)^{1/2}[\mu(T_{ij})/\mu(T_\infty)]/S_\infty{}^2 \tag{8}$$

with

$$T_{ij} = u_\infty{}^2/2R$$

This gives the ratio $\lambda_{bf}/\lambda_\infty$ numerically equal to 1.4 for the experiment.

For the transition flow regime the mean free path λ_{gw} calculated from average gas properties at the wall may also be appropriate. The ratio $\lambda_{gw}/\lambda_\infty$ has been calculated for the present case and is shown in Fig. 9. It is seen that λ_{gw} is approximately equal to λ_{bf} at the leading edge, and is equal to 6.7 mm at $x = 31.7$ mm, the point furthest downstream. Thus the so called Knudsen layer, a region within one mean free path of the plate surface, can be anything from 1.3 to 1.9 mm at the leading edge, and increases considerably at the furthest downstream point.

Figures 10–12 show the velocities, temperatures, and densities extrapolated to the wall. The extrapolations were done graphically from Figs. 6–8. It is conceivable that these properties could show a marked change within the Knudsen layer, affecting the extrapolation. Except at $x = 0$, there are no measurements within λ_∞ or λ_{bf} of the surface, but many of the downstream measurements are within λ_{gw} of the surface. Further, the close point at $x = 0$ indicates no drastic change in slope. Thus, we think that the graphical extrapolation represents, within the experimental accuracy, the actual values at the surface. Downstream of the leading edge, the measurements are well within λ_{gw} of the surface.

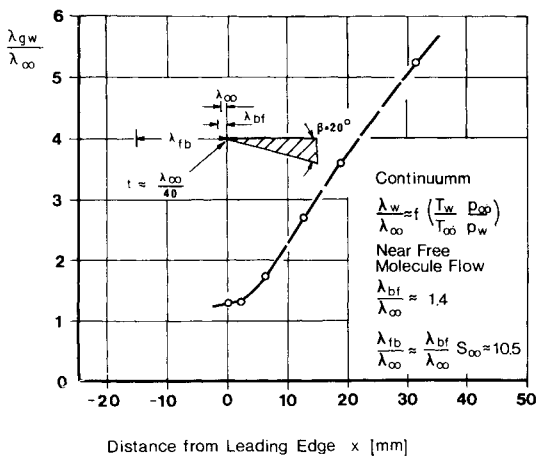

Fig. 9 Average mean free path at the wall λ_{gw} as determined from extrapolated values. $\lambda_\infty = 1.2$ mm.

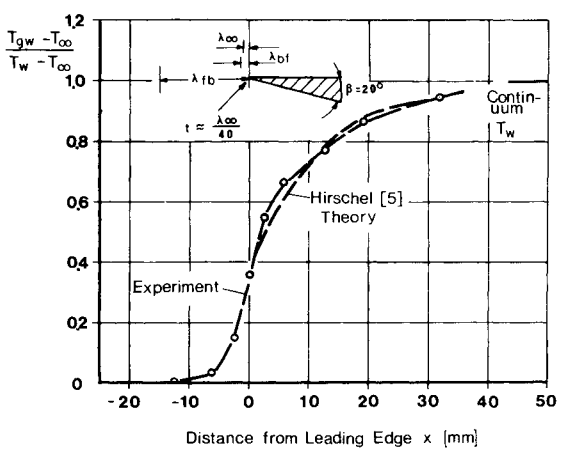

Fig. 11 Temperatures extrapolated to the wall, giving the temperature jump and comparison with Hirschel's continuum theory calculations.

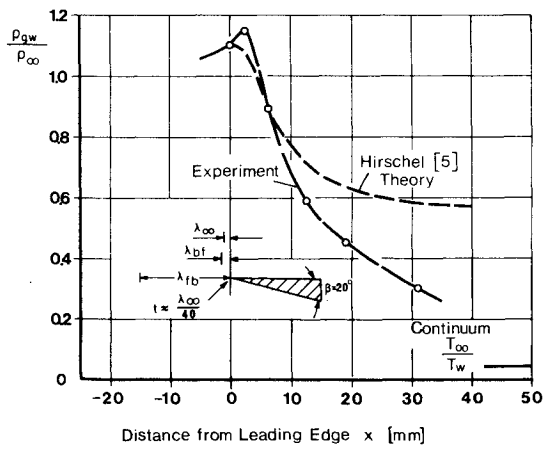

Fig. 12 Densities extrapolated to the wall and comparison with Hirschel's continuum theory calculations.

The total enthalpy of the gas is an indication of the energy content, and in Fig. 13 the enthalpy ratio H_{gw}/H_∞, extrapolated to the wall, is shown. Since the wall temperature was essentially equal to the stagnation temperature, far downstream this ratio must approach 1.0. The approximately 15% rise above 1.0 with a maximum near the leading edge is interesting, and we note in passing that the free molecular recovery temperature, for diffuse reflection, is approximately 25% greater than the stagnation temperature.[18]

V. Comparison with Available Theory

Continuum theory relations for velocity slip and temperature jump, based on the velocity and temperature profiles extrapolated to the wall, were used to determine classical energy and momentum accommodation coefficients. While these equations cannot be expected to accurately represent the extremely rarefied flow of the present experiments, the result is interesting and the derived accommodation coefficients may have some validity. As partial justification, we point out that no other theory is available. The equations were taken from the recent second-order theory of Deissler,[19] which required the first and second derivatives of U and T, extrapolated to the wall. These were determined graphically from the data of Figs. 6 and 7, and the resulting values of energy accommodation coefficient α and the tangential momentum accommodation coefficient σ are shown in Fig. 14. Both λ_{bf} and λ_{gw} (from Fig. 9) were used, which resulted in quite different values of α and σ further downstream. We note that the difference between Deissler's solution and the first order

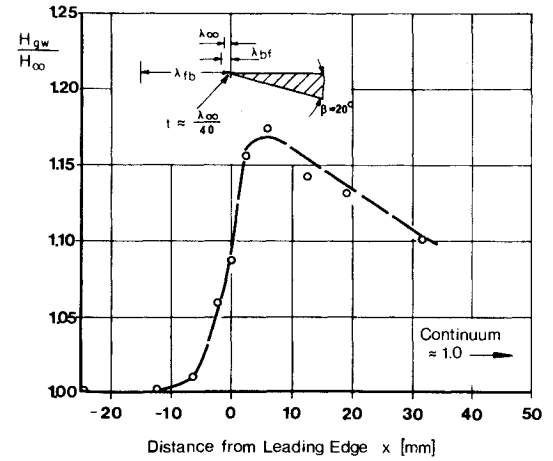

Fig. 13 Total enthalpy extrapolated to the wall.

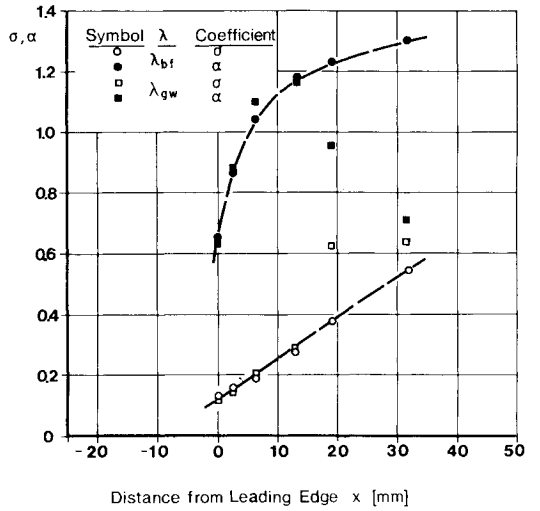

Fig. 14 Momentum and energy accommodation coefficients as calculated from the experimental data using a continuum theory. Results shown based on both λ_{bf} and λ_{gw}.

slip and jump relations as given by Schaaf and Chambre[18] are relatively small, with the second derivatives contributing only about 20%.

The generally low value of momentum accommodation near the leading edge is obvious from the raw velocity spectra, in which the molecules reflected from the plate can be approximately separated from the freestream molecules. However, there must be considerable doubt concerning absolute values as low as 0.2. The energy accommodation near the leading edge is also consistent with the value of T_2 of the bimodal fit. However, the rise to a value greater than unity downstream is likely incorrect, partly because T_2 from the bimodal fit never exceeds T_0, partly because of general theoretical considerations, and partly from more direct experimental measurements of α.

Molecular beam measurements of momentum and thermal accommodation of gases on so called "engineering surfaces"

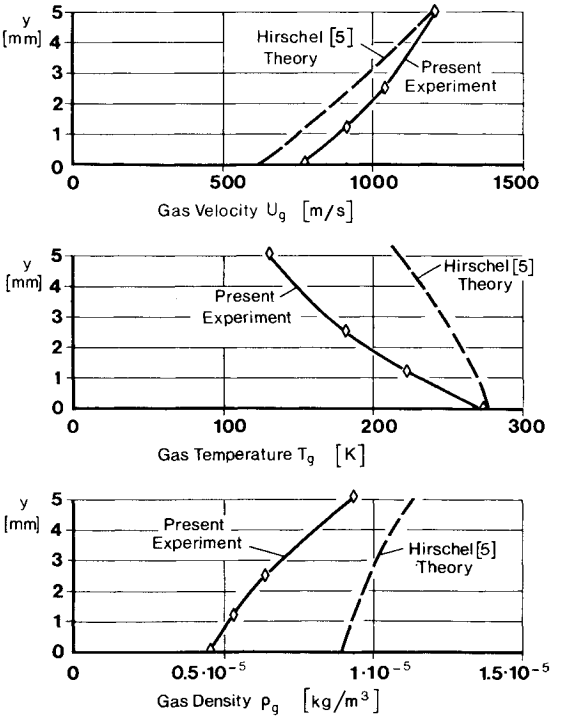

Fig. 15 Comparison of the experimental flowfield at $x = 31.7$ mm with Hirschel's continuum theory calculations.

generally give values closer to unity. In partial justification of the above evidence for a low value of the momentum accommodation coefficient, we note that near the leading edge the incident molecules strike the surface at very shallow angles. Especially in the case of a light, inert gas such as helium with low absorption potential, this would be expected to lead more nearly to specular reflection. This also accounts in principle for the increasing value of σ further downstream.

Hirschel[5] has developed a finite-difference numerical technique for the hypersonic slip-flow boundary layer. Solutions have been obtained (Hirschel, private communication) for the conditions of this experiment, using the measured values of T and U at the leading edge and the freestream values as boundary conditions, and the accommodation coefficients shown in Fig. 14. The values of U_{gw}, T_{gw}, and ρ_{gw} extrapolated to the wall are shown compared to the measurements in Figs. 10–12, where, except for T_{gw}, the agreement is not too good. In Fig. 15 the theory is compared with the flowfield data far downstream at $x = 31.7$ mm, again showing relatively poor agreement. Our general conclusion is that a continuum theory, or even a modified continuum theory, is not adequate to predict the macroscopic properties of the flowfield in the transition flow regime.

VI. Summary

Experimental measurements of the velocity distribution function within a few mean free paths of the leading edge of a flat plate in hypersonic helium flow have been obtained. The macroscopic properties velocity, temperature, and density have been calculated and are presented in graphical form downstream of the leading edge and close to the plate. An attempt to obtain the tangential momentum and energy accommodation coefficients, through use of continuum theory, was made. Based on this, plus qualitative observation of the data, it was concluded that the tangential momentum accommodation coefficient was quite small near the leading edge, and markedly increased downstream. The energy accommodation coefficient may also be less than unity near the leading edge. A direct comparison with a continuum numerical solution indicated rather poor agreement.

It appears that direct comparison with kinetic theory solutions, such as the Monte-Carlo type, may be the only satisfactory way to extract information on the molecule-surface interactions. The distribution function data are available, and we hope that future comparison will be made.

References

[1] Oguchi, H., "Shock Wave and Viscous Layer Structure in a Rarefied Hypersonic Flow near the Leading Edge of a Sharp Flat Plate," ISAS Rept. 418, Vol. 32, No. 11, 1967, Institute of Space and Aeronatucal Science, Univ. of Tokyo, Tokyo, Japan.

[2] Chow, W. L., "Hypersonic Rarefied Flow Past the Sharp Leading Edge of a Flat Plate," *AIAA Journal*, Vol. 5, No. 9, Sept. 1967, pp. 1549–1557.

[3] Shorenstein, M. L. and Probstein, R. F., "The Hypersonic Leading Edge Problem," *AIAA Journal*, Vol. 6, No. 10, Oct. 1968, pp. 1898–1906.

[4] Rudman, S. and Rubin, S. G., "Hypersonic Viscous Flow over Slender Bodies with Sharp Leading Edges," *AIAA Journal*, Vol. 6, No. 10, Oct. 1968, pp. 1883–1890.

[5] Hirschel, E. H., "The Influence of the Accommodation Coefficients on the Flow Variables in the Viscous Interaction Region of a Hypersonic-Slip Flow Boundary Layer," Paper presented at the 8th International Rarefied Gas Dynamics Symposium, Stanford, Calif., 1972.

[6] Huang, A. B. and Hwang, P. F., "Kinetic Theory of the Sharp Leading Edge Problem: II—Hypersonic Flow," IAF Paper RE 63, 1968, 19th Congress of the International Astronautical Federation, New York.

[7] Vogenitz, F. W., Broadwell, J. E., and Bird, G. A., "Leading Edge Flow by the Monte Carlo Simulation Technique," *AIAA Journal*, Vol. 8, No. 3, March 1970, pp. 504–510.

[8] Dyer, T. M. and Smith, J. A., "Upstream Influence in a Rarefied Hypersonic Stream," 8th International Rarefied Gas Dynamics Symposium, Stanford, Calif., 1972.

[9] De Geyter, F., Smolderen, J. J., and Wendt, J. F., "Influence of Leading Edge Geometry on Upstream Density Disturbances in Hypersonic Flow," 8th International Rarefied Gas Dynamics Symposium, Stanford, Calif., 1972.

[10] Becker, M., "Die Ebene Platte in Hypersonischer Strömung Geringer Dichte—Experimentelle Untersuchungen im Stossformierungs- und Übergangsgebiet," *Deutsche Luft- und Raumfahrt*, Forschungsbericht DLR FB 70–79, 1970.

[11] Ashkenas, H. and Sherman, F. S., "The Structure and Utilization of Supersonic Free Jets in Low Density Wind Tunnels," *Rarefied Gas Dynamics*, Suppl. 3, Vol. II, edited by J. H. de Leeuw, Academic Press, New York, 1966, pp. 84–105.

[12] Cattolica, R., "An Experimental Study of Translational Non-Equilibrium in Free Jet Expansions," Fluid Mechanics Rept. FM-72-6, Univ. of California, Berkeley, Calif.

[13] Muntz, E. P., "Molecular Velocity Distribution-Function Measurements in a Flowing Gas," *Physics of Fluids*, Vol. 11, No. 1, 1968, pp. 64–76.

[14] Schweiger, G., Wanders, K., and Becker, M., "Influence of Electron-Beam Blunt-Body Interactions on Density Measurements in Transition Flow," 8th International Rarefied Gas Dynamics Symposium, Stanford, Calif., 1972; also *Deutsche Luft- und Raumfahrt*, Forschungsbericht DLR FB 73-08, 1973.

[15] Robben, F. and Talbot, L., "Measurement of Shock Wave Thickness by the Electron Beam Fluorescence Method," *Physics of Fluids*, Vol. 9, No. 4, 1966, pp. 633–643.

[16] Keesom, W. H., *Helium*, Elsevier, New York, 1942.

[17] Hamel, B. B. and Cooper, A. L., "A First Collision Theory of the Hyperthermal Leading Edge Problem," *Rarefied Gas Dynamics*, Suppl. 5, Vol. I, edited by L. Trilling and H. Y. Wachman, Academic Press, New York, 1969, pp. 433–440.

[18] Schaaf, S. A. and Chambre, P. L., *Flow of Rarefied Gases*, Princeton University Press, Princeton, N.J., 1961.

[19] Deissler, R. G., "An Analysis of Second Order Slip Flow and Temperature Jump Boundary Condition for Rarefied Gases," *International Journal of Heat and Mass Transfer*, Vol. 7, 1964, pp. 681–694.